Title

Structural dissection of ergosterol metabolism reveals a pathway optimized for membrane phase separation.

Journal

Science Advances, 11(17)

Authors

Juarez-Contreras, Israel

Lopes, Laura

Holt, Jamie

et al.

Publication Date

2025-04-25

DOI

10.1126/sciadv.adu7190

BIOPHYSICS

Structural dissection of ergosterol metabolism reveals a pathway optimized for membrane phase separation

Israel Juarez-Contreras[1], Laura J. S. Lopes[2], Jamie Holt[1], Lorena Yu-Liao[1], Katherine O'Shea[1], Jose Ruiz-Ruiz[1], Alexander Sodt[2], Itay Budin[1]*

Sterols are among the most abundant lipids in eukaryotic cells yet are synthesized through notoriously long metabolic pathways. It has been proposed that the molecular evolution of such pathways must have required each step to increase the capacity of its product to condense and order phospholipids. Here, we carry out a systematic analysis of the ergosterol pathway that leverages the yeast vacuole's capacity to phase separate into ordered membrane domains. In the post-synthetic steps specific to ergosterol biosynthesis, we find that successive modifications act to oscillate ordering capacity, settling on a level that supports phase separation while retaining fluidity of the resulting domains. Simulations carried out with each intermediate showed how conformers in the sterol's alkyl tail are capable of modulating long-range ordering of phospholipids, which could underlie changes in phase behavior. Our results indicate that the complexity of sterol metabolism could have resulted from the need to balance lipid interactions required for membrane organization.

INTRODUCTION

Sterols are polycyclic triterpenoid lipids that are hallmarks of eukaryotic cell membranes. Canonical structural roles for sterols are based on their ability to condense the hydrocarbon chains of neighboring phospholipids, thereby ordering bilayers in a concentration-dependent manner (*1*). While this function might be universal, it does not explain the chemical diversity in sterol metabolism among eukaryotic lineages (*2*). Synthesis of sterols is metabolically complex, with the most common pathways featuring 10 or 11 distinct steps, several of which are oxygen dependent. The recent discovery of protosterols in the fossil record corresponding to each of the crown group eukaryotes supports a model in which the emergence of sterol metabolism occurred during the early evolution of eukaryotes, likely alongside increasing oxygen levels during the Tonian period (*3*). While the initial steps for each pathway are similar, their subsequent diversification suggests disparate selective pressures during eukaryotic evolution (*4*). In the case of ergosterol, the most common fungal sterol, early steps are shared with cholesterol biosynthesis in metazoans, while later steps are unique and differentiate the pathway's final product (Fig. 1A).

The complexity of sterol biosynthesis has long motivated models for understanding the evolution of metabolic pathways. On the basis of measurements of membrane permeability, acyl chain ordering parameters by NMR, and microviscosity estimates by fluorescence anisotropy, Bloch and colleagues first observed that cholesterol has a stronger capacity to order phosphatidylcholine (PC) bilayers than its first precursor lanosterol, with demethylated cholesterol precursors in the pathway showing intermediate effects (*5*–*7*). These experiments led to the proposal that sterol metabolism has evolved primarily to increase membrane ordering for improved barrier functions of cell membranes (*8*). In the Bloch hypothesis, each successive pathway intermediate is expected to show superior ordering capability, thereby explaining their sequential adoption during the evolution of the pathway. Such an optimization is best understood through changes in the bifacial topology of the sterol ring system after lanosterol synthesis: One plane (the α-face) is demethylated three times for optimal van der Waals interactions with neighboring phospholipid chains, while the other (the β-face) retains two vestigial methyl groups that contribute to its orientation in the bilayer (*9*, *10*). These demethylations are conserved across pathways. However, subsequent steps that are unique to each pathway have not been explained by the Bloch hypothesis, such as the generation of the methylated tail in ergosterol (*11*) and plant phytosterols (*12*). These sterols have been observed to show inferior ordering capabilities compared to cholesterol (*8*, *13*), leading to models in which factors, such as temperature (*8*), desiccation (*14*), ultraviolet irradiation (*3*), could have instead driven their evolution.

The Bloch hypothesis was formulated before the discovery that sterols are required to support lateral membrane heterogeneity, a process that depends on their interaction with multiple lipids. When included in mixtures of high– and low–melting temperature phospholipids or sphingolipids, sterols can cause membranes to phase separation into liquid ordered (L_o) and liquid disordered (L_d) domains (Fig. 1C) (*15*). Colloquially termed lipid rafts, this emergent property has been well characterized in model membrane systems, such as giant unilamellar vesicles (GUVs) (*16*). Without sterols, high–melting temperature lipids can still demix but form gel-like, solid domains whose reduced dynamics might preclude biological functions (*17*). While sterols are necessary for fluid membrane phase separation, the specific structural requirements for this process have not been elucidated. The α-face methylated sterol lanosterol does not support domains in model membranes (*18*), indicating that ordering capacity is required for domain formation. However, even late-stage intermediates, such as 7-dehydrocholesterol that accumulates in patients with Smith-Lemli-Opitz syndrome, can also show altered domain forming capacity (*19*). A set of sterol derivatives, classified as inhibitor sterols, has also been observed to prevent liquid domain formation, instead disrupting phase separation (*20*) or favoring the formation of solid domains (*18*). These studies suggest that membrane phase separation is sensitive to specific chemical features of sterols, but more systematic analyses have been hampered by the limited availability of sterol intermediates.

[1]Department of Chemistry and Biochemistry, University of California San Diego, La Jolla, CA 92093, USA. [2]Unit on Membrane Chemical Physics, Eunice Kennedy Shriver National Institute of Child Health and Human Development, 29 Lincoln Drive, Bethesda, MD 20892, USA.
*Corresponding author. Email: ibudin@ucsd.edu

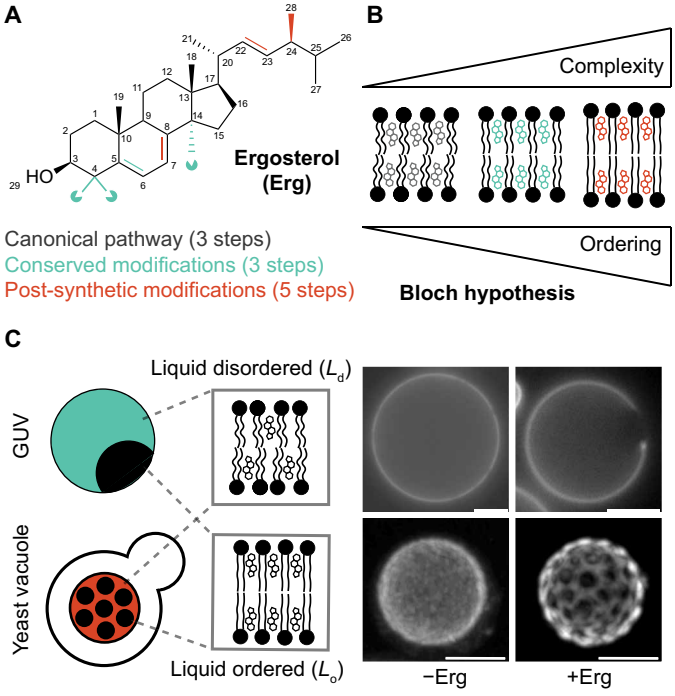

Fig. 1. Biosynthesis of sterols and their role in membrane phase separation. (**A**) Chemical structure of the fungal sterol ergosterol, with highlighted modifications grouped according to their occurrence during its metabolism. The canonical sterol pathway yields the ring system, conserved modifications among fungi and animals result in demethylation of α-face carbons (indicated by a Pacman symbol at removed methyl groups), while post-synthetic modifications exclusive to ergosterol primarily remodel the alkyl chain. (**B**) Schematic of the Bloch hypothesis, which proposes that the capacity for sterols to condense and order phospholipids rose continuously along the pathway. (**C**) Liquid phase separation between L_d and L_o domains is a sterol-dependent membrane property that can be observed in both synthetic systems [giant unilamellar vesicle (GUV)] and in cells (the yeast vacuole). In both GUVs and vacuoles, changes in ergosterol concentrations drive the loss or appearance of L_o/L_d phase separation. Shown are 3:1 dioleoyl PC (DOPC):dipalmitoyl PC (DPPC) GUVs prepared with 0 (left) and 20 mol % (right) ergosterol (top) and yeast vacuoles from an ergosterol depleted strain (*ERG9* knockdown, left) compared to WT (right). Scale bars, 5 μm.

Although best understood in model systems, membrane phase separation is also thought to be relevant for molecular organization in vivo. In mammalian cells, domains in the plasma membrane are small and dynamic, making systematic characterization challenging (*21*). An alternative model system is the vacuole of yeast cells (Fig. 1C). Upon nutritional stress or transition of cells into the stationary growth stage, vacuole membranes organize into micron-scale domains (*22*). These structures can act as internalization sites for neutral lipid stores that help cells survive under these conditions (*23*). Vacuole domains show hallmarks of phase separation in model membranes: fluid-like mobility, a tendency to coalesce upon collision, and a characteristic miscibility temperature above which they reversibly dissolve (*24*). Domain formation during early stationary stage growth corresponds to an increase in membrane ergosterol composition, alongside that of high–melting temperature sphingolipids (*25*), and domains from isolated vacuoles are sensitive to sterol depletion (*26*), as they are in vesicles (*27*). Genetic and chemical depletion of ergosterol from cells also prevents vacuole domains from forming in cells (*22*). Alterations in the abundance and structure of vacuole sphingolipids modulate domain structure (*25*), suggesting that a balance of distinct lipid species is required for robust phase separation of liquid domains.

Here, we take advantage of the yeast vacuole to investigate the physicochemical requirements for sterol-driven membrane phase separation. Motivated by the Bloch hypothesis, we asked whether successive intermediates in the ergosterol pathway exhibit improved capacities to form ordered domains. Extraction of sterol intermediates from strains allowed us to identify these features and measure their interactions with phospholipids, which was further explored with all-atom simulations. Together, these data uncover a pathway that does not maximize the condensation capacity but rather balances it to support phase separation of fluid domains.

RESULTS

Genetic modulation of early-stage modifications and effects on phase separation

To directly test the function of intermediates, we generated yeast strains to systematically modify sterol composition in cells. Early stages of the pathway, shared with cholesterol synthesis in metazoans, form the initial cyclized product lanosterol and its subsequent demethylation into zymosterol. These steps include the condensation of two farnesyl pyrophosphate into squalene by Erg9, squalene oxidation into 2,3-oxidosqualene by Erg1, and the formation of lanosterol by the cyclase Erg7. Lanosterol is demethylated by Erg11 into 4,4-dimethylcholesta-8,14,24-trienol [or follicular fluid meiosis--activating sterol (FF-MAS)], reduced into 4,4-dimethylzymosterol by Erg24, and again demethylated by the coordinated activities of the Erg25, Erg26, and Erg27 into zymosterol. While these steps are all essential for viability, yeast can tolerate large reductions in ergosterol abundance, which naturally occurs during microaerobic fermentation. We thus used a promoter replacement strategy to place expression of their coding genes under control of supplemental doxycycline (P_{tetoff}) or methionine (P_{MET}) (Fig. 2A). The resulting strains are summarized in table S1.

We hypothesized that repression of specific *ERG* genes would allow sufficient expression for viability under laboratory growth conditions while strongly reducing the accumulation of the subsequent biosynthetic product. To test this, we measured sterol compositions of cells grown under vacuole domain-forming conditions under continual repression. The resulting profiles (Fig. 2B) changed from wild-type (WT) cells as expected based on the genes targeted, with an accumulation of the upstream intermediate in the pathway. For *ERG24* knockdown (P_{tetoff}-*ERG24*), accumulation of the expected intermediate FF-MAS was accompanied by a derivative (ignosterol) previously observed in cells treated with antifungal Amorolfine (*28*). All strains retained residual ergosterol, presumably supporting their viability, but at levels <10% of WT cells except for P_{tetoff}-*ERG24*.

We next tested the effects of accumulating early-stage intermediates on ordered domain formation in the yeast vacuole (Fig. 2C and fig. S1A). Growth under metabolic restriction (0.4% glucose) drives vacuole membrane phase separation in most cells imaged using the L_d marker Pho8–green fluorescent protein (GFP). Analysis of cells by confocal microscopy can thus be used to quantify the frequency of cells, showing large-scale, visible vacuole membrane heterogeneity. This analysis is limited by the resolution of confocal microscopy and thus does not detect nanoscopic domains below ~200 nm in

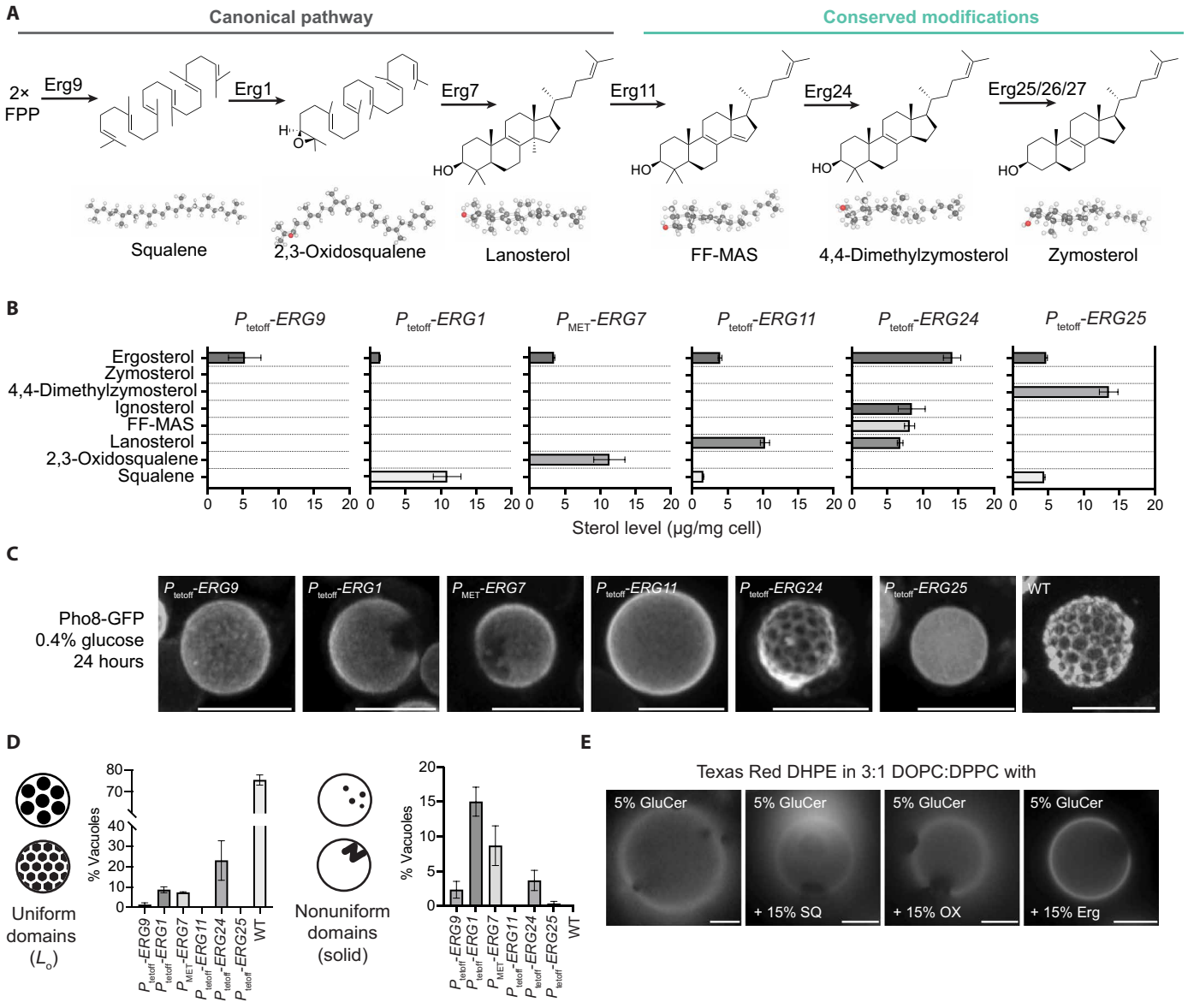

Fig. 2. Early-stage intermediates show limited capacity for L_o/L_d phase separation. (**A**) Schematic of canonical sterol-forming steps and conserved modifications, shared between ergosterol and cholesterol synthesis. FPP, farnesyl pyrophosphate. (**B**) Sterol composition of knockdowns in each early-stage step as measured by gas chromatography–mass spectrometry (GC-MS). $n = 3$ independent cultures; error bars = SD. (**C**) Representative vacuole morphologies for each strain, shown as three-dimensional (3D) projections generated from confocal *z*-stacks. Among mutants, only *ERG24* knockdown still yields robust L_o domain formation, likely because of increased residual ergosterol content. Scale bars, 5 μm. Corresponding wide-field images with multiple cells are shown in fig. S1A. (**D**) Quantification of uniform (L_o) and nonuniform (solid) domain formation frequency in stationary phase cells. Gel-like domains are abundant in mutants that accumulated squalene or 2,3-oxidosqualene. $n = 3$ independent cultures with $n > 100$ cells each; error bars = SEM. (**E**) Early-stage uncyclized intermediates squalene (SQ) and 2,3-oxidosqualene (OX) at 15 mol % cause expansion of solid or gel-like domains formed by 5 mol % of the glycosphingolipid glucosylceramide (GlcCer) in 3:1 DOPC:DPPC GUVs. In contrast, ergosterol supports fluid L_o/L_d domains (right). The presence of multiple domains in GUVs allowed to equilibrate below the mixing temperatures indicates non-fluid domains that do not coalesce. Scale bars, 5 μm.

diameter (fig. S1B). Using this pipeline, all early-stage knockdowns showed reductions in domain formation, supporting the essential role of ergosterol in this process (Fig. 2D). Compared to *ERG9* knockdown cells, which contained very few phase-separated vacuoles, *ERG1* and *ERG7* knockdowns that accumulate linear precursors (squalene and 2,3-oxidosqualene) showed enhanced domain formation. However, these were predominantly irregularly shaped and commonly appeared as congregations of domains that are in contact with one another, yet fail to coarsen (fig. S1C), suggesting that they represented solid or gel-like domains previously observed in yeast sphingolipid mutants (*25*). Solid domains were observed in half and two-thirds of all phase-separated vacuoles in *ERG7* and *ERG1* knockdown cells, respectively. The only early-stage knockdown to support robust uniform domain formation was that for

ERG24, which accumulated FF-MAS and its derivatives. However, *ERG24* knockdown cells also contained higher amounts of ergosterol than other strains, suggesting that its phenotype was not based on the accumulated intermediates themselves. Consistent with this hypothesis, we found that FF-MAS itself does not support lateral phase separation in GUVs (fig. S2).

Given that *ERG1* and *ERG7* knockdown cells showed levels of domain formation not observed in subsequent pathway steps, we asked whether linear sterol precursors affect domain membrane formation in GUVs. In ternary mixtures with 60 mol % dioleoyl PC (DOPC) and 20 mol % dipalmitoyl PC (DPPC), we observed that both squalene and 2,3-oxidosqualene inhibit formation of L_o domains in mixtures with ergosterol (fig. S3). However, in vacuoles, the accumulation of these intermediates caused formation of irregular gel-like domains, which have been observed in membranes containing high–melting temperature glycosphingolipids (*29*). We therefore tested whether linear sterol precursors promoted phase separation in membranes containing the glucosylceramide (GlcCer), which resembles the yeast sphingolipid inositol phosphoceramide that accumulates to 5 mol % of all lipids in phase-separated vacuoles (*25*). We observed that 15 mol % of squalene or 2,3-oxidosqualene cause gel-like domains to enlarge in GUVs containing 5 mol % GlcCer (Fig. 2E). In contrast, ergosterol solubilized 5 mol % GlcCer into fluid L_o domains, analogous to the state of WT vacuoles. Thus, early sterol precursors could have roles in promoting membrane heterogeneity but, overall, lack the capacity to support liquid (L_o/L_d) phase separation as ergosterol does.

How domain formation capacity arises along the post-synthetic steps?

We next explored precursors that arise in the late-stage pathway, termed post-synthetic steps by Bloch (*8*), which are specific to ergosterol metabolism (Fig. 3A). In this part of the pathway, the alkyl tail is methylated (Erg6) and its double bond moved to the C22 (*23*) position through the successive actions of a desaturase (Erg5) and a reductase (Erg4). On the B-ring, the isomerase Erg2 converts the Δ^8 double bond to a Δ^7 one, and the desaturase Erg3 introduces an additional double bond at Δ^5. These actions lead to a final product whose B-ring is diunsaturated ($\Delta^{5,7}$) and a 6-carbon tail that is monounsaturated at C22 and methylated at C24(28).

Ergosterol's post-synthetic steps are not essential for yeast viability, so combinations of gene knockouts could be used to test the activity of the preceding precursors (Fig. 3A). Among single gene knockouts, expected sterol intermediates were the most abundant sterol in *erg6*Δ (zymosterol) and *erg4*Δ [ergosta-5,7,22,24(28)-trienol], with minor accumulation side products or derivatives, as has previously been observed (*30*). The expected products of *erg2*Δ (fecosterol), *erg3*Δ (episterol), and *erg5*Δ [ergosta-5,7,24(28)-trienol] were modified by varying degrees to alternative, noncanonical sterols by subsequent enzymes in the pathways. To isolate pure canonical intermediates, we generated an *erg5*Δ*erg4*Δ double knockout to isolate ergosta-5,7,24(28)-trienol, an *erg3*Δ*erg5*Δ*erg4*Δ triple knockout for episterol, and an *erg2*Δ*erg3*Δ*erg5*Δ*erg4*Δ quadruple knockout for pure fecosterol. However, we continued analysis of noncanonical sterol-producing strains, because they provided additional information on structure-function relationships. A metabolic map showing the products accumulating in each mutant strain analyzed is shown in fig. S4, while abundances of the canonical and noncanonical intermediates are shown in Fig. 3B and fig. S5, respectively.

Imaging of vacuoles of late-stage single knockouts showed that only *erg3*Δ and *erg5*Δ, which produce ergosta-7,22-dien-3β-ol and ergosta-5,7-dienol respectively, showed observable vacuole domains prevalent in WT cells (Fig. 3C). Among double knockouts, *erg3*Δ*erg5*Δ cells accumulating ergosta-7-en-3β-ol also showed domain capacity, but only in a few cells. Cells synthesizing zymosterol (*erg6*Δ), fecosterol (*erg2*Δ and *erg2*Δ*erg3*Δ*erg5*Δ*erg4*Δ), ergosta-7,22,24(28)-trien-3β-ol (*erg3*Δ*erg4*Δ), and ergosta-7,22,24(28)-trienol (*erg5*Δ*erg4*Δ) did not display any vacuole domains (Fig. 3D). Notably, all post-synthetic intermediates that supported vacuole domain formation lacked the C-24(28) alkyl tail unsaturation due to the activity of the C24(28) reductase Erg4. Many, but not all, late-stage mutants also showed a vacuole fragmentation phenotype as previously observed (fig. S1D) (*31*), suggesting that ergosterol structural features are required for vacuole fusion that occurs when cells enter stationary phase (*32*). Enhanced fragmentation was also apparent in early-stage knockdowns to a lesser extent (fig. S1E). Because fragmented vacuoles never showed membrane domains, vacuole fusion is likely required for domain formation. When accounting for cells containing successfully fused vacuoles, domain frequency in some mutant strains, like *erg5*Δ, approach but did not fully match those of WT cells (Fig. 3D). Vacuole domain frequency among all cells is provided in fig. S1F.

As with early-stage mutants, we asked whether observed phenotypes corresponded to domain formation capacity in model membranes. Because these intermediates are not synthetically available, we isolated sterol extracts from each strain (fig. S6) and incorporated them as a 20 mol % sterol fraction into DOPC/DPPC GUVs containing the L_d marker Texas Red dihexadecanoyl-PE (DHPE). Preparations containing sterol extracts from all the strains that consistently displayed vacuole domains (*erg3*Δ, *erg5*Δ, and WT) also showed a predominance of GUVs displaying L_o/L_d (liquid) phase separation (Fig. 4A and fig. S7). We also observed phase separation in mixtures containing sterol extracts from *erg6*Δ (zymosterol), *erg2*Δ (fecosterol), and *erg3*Δ*erg5*Δ (ergosta-7-en-3β-ol) cells, but most of the resulting domains were irregularly shaped and did not coalesce during extended (>1 hour) incubation at room temperature, indicating that they were solid (*16*). Notably, solid domains were previously observed in vesicles prepared with synthetic zymosterol, the primary sterol in *erg6*Δ extracts (*33*). No consistent phase separation was observed for the other canonical or noncanonical intermediates, although we cannot rule out that they could still support domains that require long timescales to become detectable. Overall, our analysis indicated that (i) post-synthetic intermediates preceding Erg2 activity, which contain an Δ^8 B-ring, support the formation of solid domains; (ii) intermediates with a Δ^7 B-ring but containing a C24(28) tail unsaturation (preceding Erg4 activity) do not support robust lipid demixing, similar to other low-ordering sterols like lanosterol; and (iii) sterols containing both a Δ^7 B-ring and a reduced C24(28) alkyl tail support L_o/L_d membrane phase separation (Fig. 4B).

Non-monotonic changes in condensation capacity caused by post-synthetic modifications

The Bloch hypothesis predicts that membrane ordering of phospholipid membranes imparted by each sterol intermediate should increase along the pathway. However, ergosterol, as a final product, shows poor capacity to order unsaturated phospholipids when compared to cholesterol (*34*), suggesting that this model might not hold for the fungal pathway. To test this possibility, we used sterol extracts from

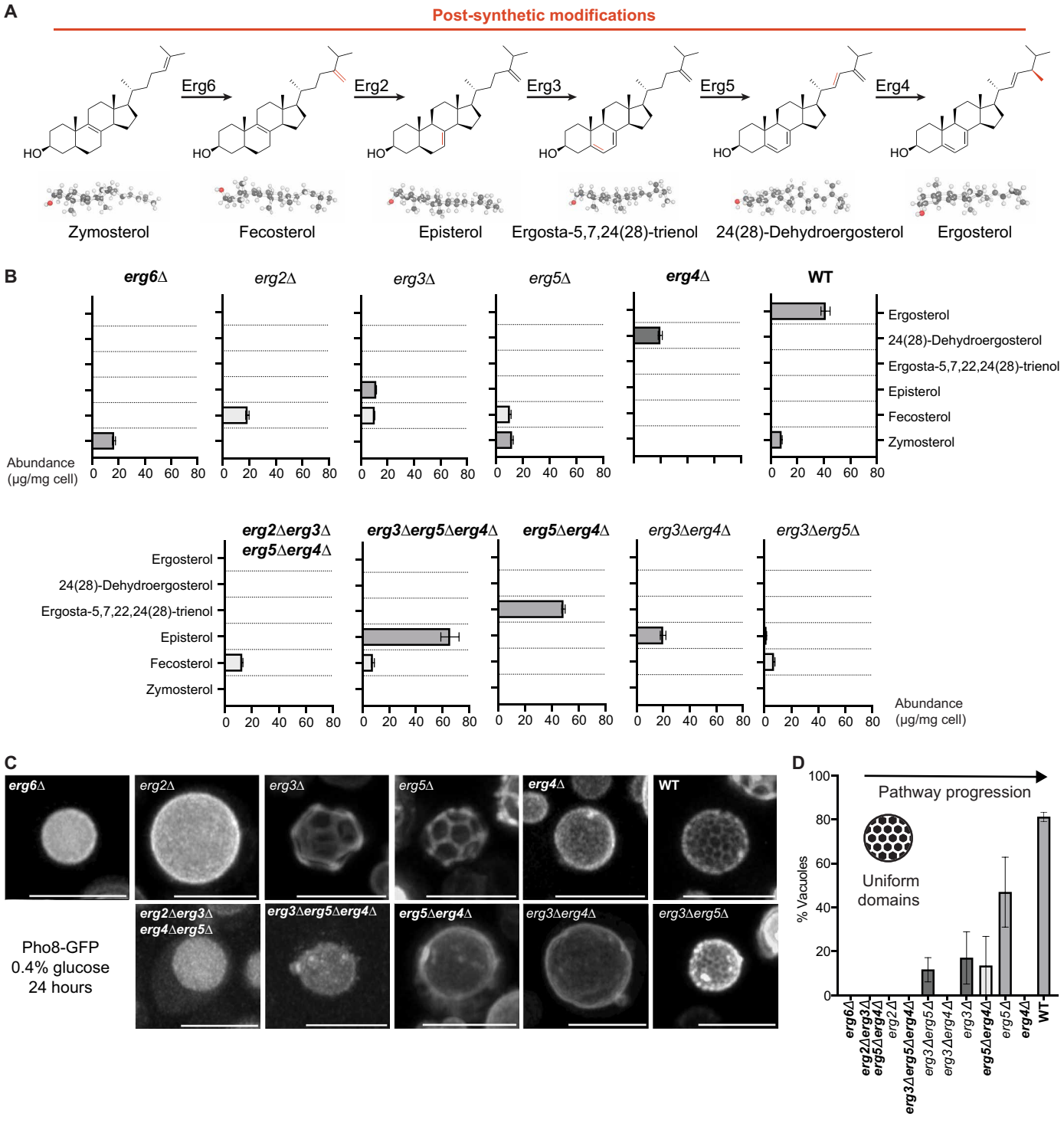

Fig. 3. Post-synthetic sterol intermediates show a non-monotonic increase in ability to support membrane phase separation. (**A**) Schematic of post-synthetic steps transforming zymosterol into ergosterol. (**B**) Sterol composition of mutants that isolate each of the post-synthetic steps as measured. Mutants in bold predominantly produce an ergosterol intermediate in the canonical pathway shown in (A), while those that are unbolded produce noncanonical intermediates as shown in fig. S4. $n = 3$ independent cultures; error bars = SD. (**C**) Representative Pho8-GFP distribution in each strain shown as 3D projections generated from Airyscan confocal *z*-stacks. Only *erg3*Δ, *erg5*Δ, and *erg3*Δ*erg5*Δ and WT cells show robust domain formation in the vacuole, which is most abundant in the latter that synthesizes ergosterol. Scale bars, 5 μm. Wider-field images with multiple cells are shown in fig. S1A. (**D**) Quantification of domain formation frequency in fused vacuoles of stationary phase cells in 0.4% glucose. Mutants in bold predominantly produce an intermediate in the canonical pathway shown in (A). Ordering of strains and arrow indicating pathway progression correspond to accumulated intermediates, showing each canonical intermediate in order (bold), followed by their matching noncanonical products formed by Erg3, Erg5, and/or Erg4 reactions. Domains arise along the post-synthetic steps. $n = 3$ independent cultures; error bars = SEM.

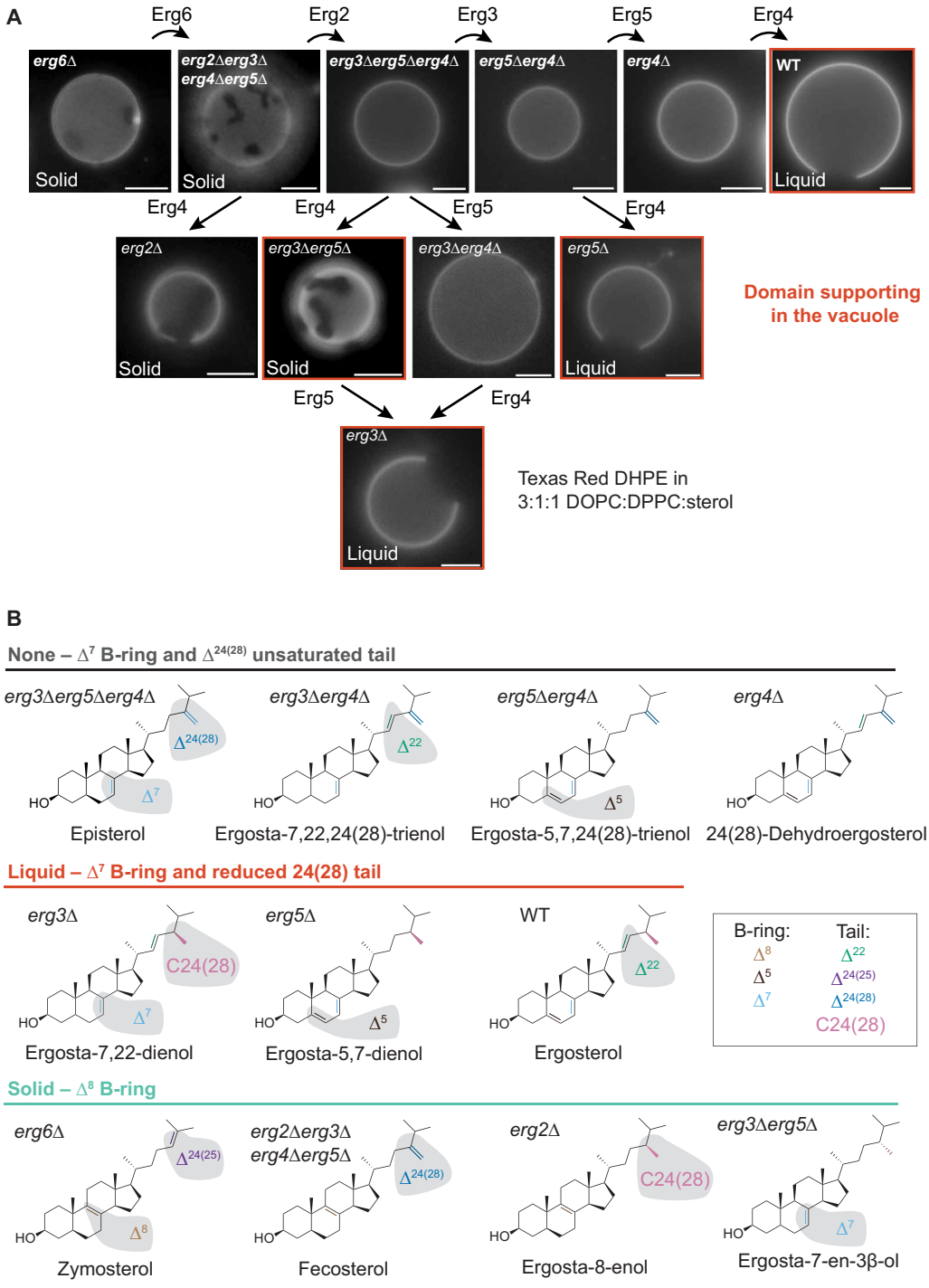

Fig. 4. Structural features of ergosterol intermediates that support membrane domains. (**A**) Micrographs of GUVs composed of a 3:1 ratio of DOPC:DPPC with 20 mol % of sterols extracted from each post-synthetic mutant. GUVs contain the L_d marker Texas Red DHPE and domains were allowed to coalesce at room temperature for >1 hour. Micrographs are arranged by their metabolic basis, with enzyme activity that converts their dominant sterol species shown through reaction arrows. In mixtures that support phase separation, the type is indicated by the inset text. Liquid domains are characterized by their capacity to coalesce. Extracts corresponding to yeast strains that show vacuole domains are highlighted in orange. The names of strains accumulating canonical intermediates are bolded. Quantification of domain type frequency across preparations is provided in fig. S7. Scale bars, 5 μm. (**B**) Structures of the predominant sterols from each strain categorized by their ability to either promote gel-like domains (solid), L_o domains (liquid), or no domains (none) in GUVs. B-ring and tail structural features are color coded to highlight differences in each category. Solid domain-promoting sterols contain a Δ^8 B-ring, which is isomerized by Erg2, with the exception of ergosta-7-en-3β-ol that showed solid domains. Sterols that cannot form domains under these conditions feature a Δ^7 B-ring and have an unsaturated branched tail. Sterols that form liquid (L_o) domains have a Δ^7 B-ring and a tail that is reduced at C24(28) by Erg4.

the post-synthetic mutants and incorporated them into 1-palmiyoyl-2-oleoyl-PC (POPC) vesicles at a fixed stoichiometry (20 mol %) and assayed membrane ordering at 30°C by the change in generalized polarization (ΔGP) of C-Laurdan compared to sterol-free POPC (Fig. 5A). In liposomes prepared from extracts of canonical intermediates, ΔGP was highest for early-stage intermediates (zymosterol, *erg6*Δ; and fecosterol, *erg2*Δ*erg3*Δ*erg5*Δ*erg4*Δ) and steadily decreased as the pathway progressed. Thus, intermediates that best support L_o/L_d phase separation show low capacity to order membranes composed of the unsaturated phospholipids.

Given that ergosterol has been observed to have stronger ordering effects on saturated phospholipids (*34*, *35*), we carried out identical experiments using saturated dimyristoyl PC (DMPC) mixtures vesicles (Fig. 5B). Like for POPC liposomes, we observed the highest ΔGP for early post-synthetic intermediates, consistent with previous measurements of zymosterol (*36*). In later steps, however, the ΔGP DMPC partially recovers for ergosterol compared to its immediate precursors, ergosta-5,7,24(28)-trienol (*erg5*Δ*erg4*Δ) or 24(28)-dehydroergosterol (*erg4*Δ). Laurdan GP of DMPC with each sterol at 30°C was correlated [coefficient of determination (R^2) = 0.90] with the miscibility temperatures of the mixtures, as measured using fluorescence polarization of diphenylhexatriene (DPH) (fig. S8) or with Laurdan GP (fig. S9). When we calculated the difference in GP between POPC and DMPC liposomes containing sterol extracts, we observed that ergosterol had the largest difference between the unsaturated and unsaturated systems (Fig. 5C). In general, extracts that allowed for L_o/L_d phase separation in vacuoles and GUVs, such as *erg3*Δ, *erg5*Δ, and WT, also had large GP differences between DMPC and POPC systems. Thus, post-synthetic modifications do not uniformly increase ordering but rather oscillate it to maintain differences between sterol-containing unsaturated and saturated lipid membranes. This dynamic corresponds to the loss of solid domains and the reappearance of liquid domains along the pathway (Fig. 5D).

The structural basis for sterol ordering explored by all-atom simulations

We were surprised by the capacity of small structural changes in ergosterol precursors, B-ring and alkyl chain unsaturations, to cause large changes in membrane ordering capacity. To further investigate the mechanisms underlying these effects, we used molecular simulations of sterol-containing bilayers using the CHARMM36 all-atom force field. For each canonical post-synthetic intermediate, we generated and refined structural models, which were then incorporated into bilayers of DMPC at 20 mol % (Fig. 6A). Using these simulations, we calculated changes in acyl chain ordering parameters (ΔS_{CD}, averaged over acyl chain carbons 4 to 10) of DMPC chains relative to sterol-free systems (Fig. 6B). Overall, the correlation between ΔS_{CD} from simulations and miscibility temperatures measured experimentally for each extract in DMPC was robust (R^2 = 0.92; Fig. 6C), supporting the use of CHARMM36 to interrogate sterol structure-function.

As in experiments, we found a substantial difference in ordering capacity among post-synthetic intermediates. Early-stage sterols (zymosterol or *erg6*Δ, and fecosterol or *erg2*Δ) showed high DMPC ordering capacities, mid-stage sterols [episterol or *erg5*Δ, and 24(28)-dehydroergosterol or *erg4*Δ], showed low ordering capacity, and ergosterol displayed an intermediate level (Fig. 6B). This non-monotonic trend mirrored what was observed in membrane ordering experiments (Fig. 5). Visualization of these systems showed

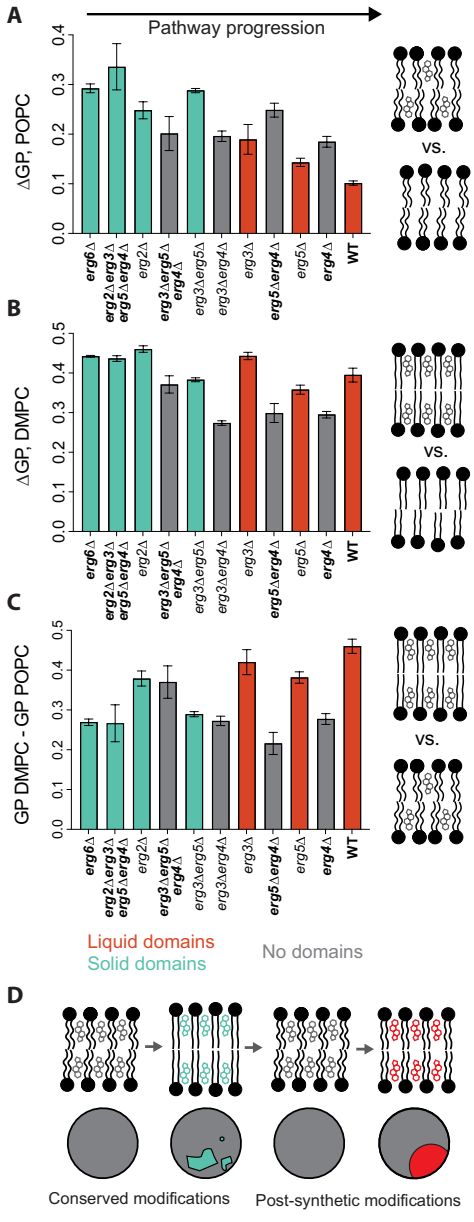

Fig. 5. Ordering capacities of ergosterol intermediates that support domains. (**A**) The change in Laurdan GP for unsaturated (POPC) phospholipid vesicles upon incorporation of 20 mol % sterol was measured for extracts from each of the post-synthetic mutants at 30°C. ΔGP was calculated by subtracting the GP of POPC without sterol (−0.245 ± 0.011) from that measured with each of the sterol-containing samples. Mutants that accumulate canonical intermediates are indicated with bolded names. Strains whose sterols support membrane domains in GUVs are highlighted according to the type of domain. Liquid domain supporting sterols show low condensation of unsaturated phospholipids. n = 3 independent liposome preparations; error bars = SD. (**B**) The change in GP for saturated (DMPC) phospholipid vesicles upon incorporation of 20 mol % sterol at 30°C. Domain supporting sterols show moderate to high ordering of saturated phospholipids, which corresponds to the miscibility temperatures of the mixtures (fig. S8C). The GP value for pure DMPC was −0.078 ± 0.018. (**C**) The difference in GP between DMPC and POPC systems, both containing 20 mol % sterol, is largest for the ergosterol intermediates that also support liquid phase separation. (**D**) A model highlighting non-monotonic changes in ordering capacity in the ergosterol pathway and relationship to phase separation of coexisting domains of different types.

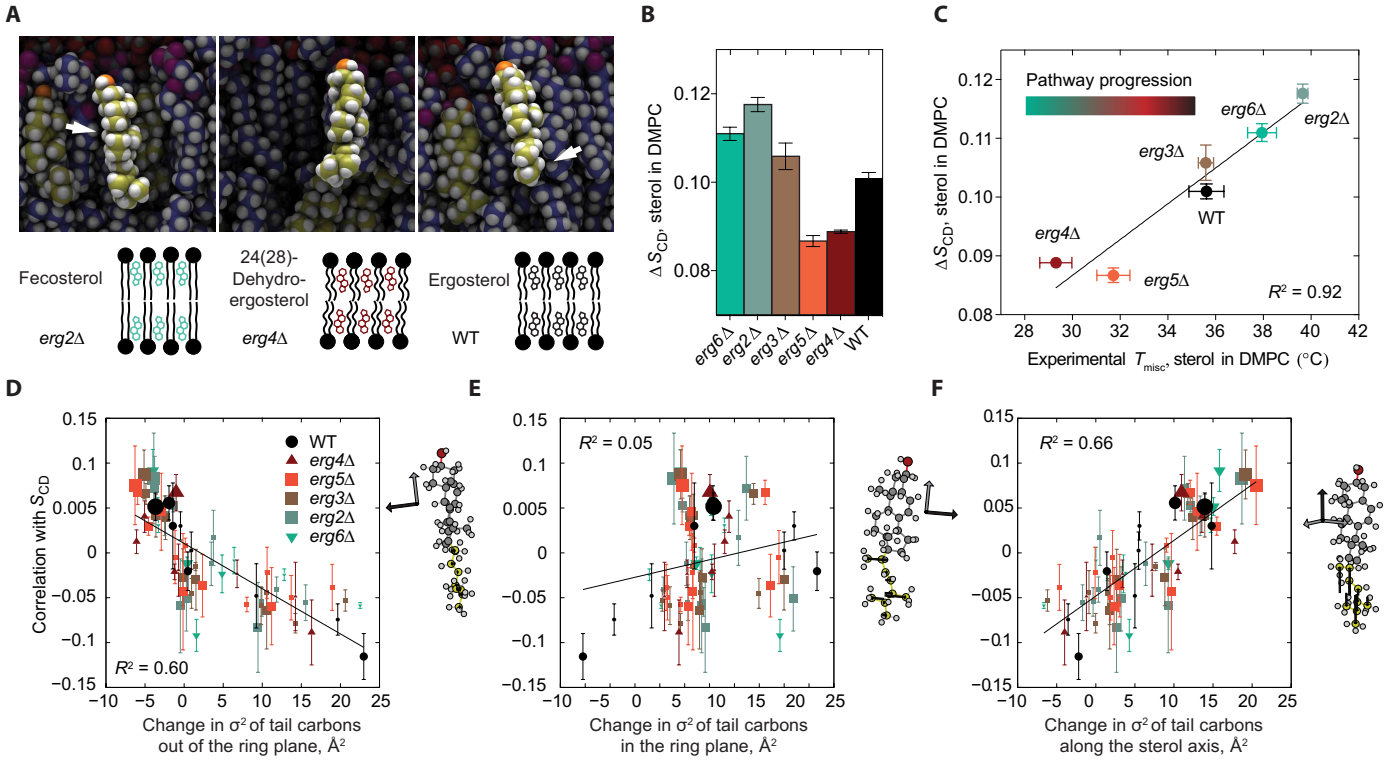

Fig. 6. Atomistic models for phospholipid condensation by post-synthetic intermediates. (**A**) Examples of representative structures of post-synthetic sterol intermediates in all-atom simulations. The arrow in the fecosterol image highlights the smooth α-face of the ring system, while that in the ergosterol image highlights the extended alkyl tail. (**B**) Increase in acyl chain ordering parameter (ΔS_{CD}) in with 20 mol % post-synthetic intermediates compared to pure DMPC. Systems are referred to by gene deletion corresponding to the subsequent enzyme in the pathway that acts upon them, e.g., *erg2*Δ for fecosterol extracted from *erg2*Δ*erg3*Δ*erg5*Δ*erg4*Δ, *erg3*Δ for episterol from *erg3*Δ*erg5*Δ*erg4*Δ, and *erg5*Δ ergosta-5,7,24(28)-trienol from *erg5*Δ*erg4*Δ. (**C**) ΔS_{CD} in simulations correlates with measured miscibility temperatures (T_{misc}) of the same mixtures ($R^2 = 0.915$). Sterol-free DMPC has a T_{misc} of 24°C. Error bars = SD. (**D** to **F**), Correlation of S_{CD} with tail configuration shape relative to the sterol ring. For each dynamic conformation, 3D axes (indicated by the black axis in each panel) are determined by the moments of inertia of the ring system. Displacements of tail carbons are measured for each 3D axis, squared, and summed. The deviation of that sum from the mean is plotted on the *x* axis. The size of each mark represents their relative abundance for that specific sterol, which is indicated by its color and shape. Plotted are deviations out of the axis out of the ring plane (D), within the axis in the ring plane but perpendicular to the sterol long axis (E), and along the sterol long axis (F). Small deviations out of the ring plane are positively correlated with order, as are extensions along the axis. There is no correlation for deviations within the ring plane. These features are consistent with an extended tail conformation correlating with ordering. Error bars = SD of three independent simulations.

clear differences in the sterol conformations, particularly in the alkyl tail that is remodeled during the post-synthetic steps (Fig. 6A). To quantify these conformational changes, we correlated each sterol conformation, measured via each dihedral angle of the sterol tail, to the instantaneous total bilayer order in each frame of the simulations. This analysis showed that ordering was correlated with low deviations of the tail carbons out of the plane of the sterol ring (Fig. 6D). In contrast, there was no correlation between ordering and with variations along the ring plane (Fig. 6E). Ordering was also correlated with increasing extension of carbons along the sterol axis itself (Fig. 6F). Together, these results indicate that increased sterol ordering results from a more extended tail conformation in bilayers.

Long-range organization of phospholipids modulated by ergosterol metabolism

To further understand the effect of differing sterol structures on neighboring phospholipids, we analyzed the distribution of DMPC ordering (S_{CD} parameters) across the entire bilayer for each sterol system. Across all systems, the distribution of individual acyl chain S_{CD} values could be deconvolved into two peaks (fig. S10A): a tightly distributed high order population and a broader, lower order one. The former increases with the average order of the system, while the latter is largely unchanged (Fig. 7A). Unexpectedly, the differences in S_{CD} across all systems was explained entirely by the increase in frequency of the high-order configurations, as the abundance of these DMPC states was tightly correlated ($R^2 > 0.99$) with total simulated membrane ordering (Fig. 7B) and experimentally measured miscibility temperatures (fig. S10B). When we classified DMPC acyl chains by their gauche-trans isomerization, which yielded 1024 distinct classes of chain conformers, we found that only 10 chain classes present a monotonic percentage increase with increasing order. These classes all present at least seven consecutive carbons with trans conformations: XTTTTTTTTX, TGTTTTTTTX, TTTTTTTTGX, and TTTTTTTGTG, with X being either gauche (G) or trans (T) (data S2). Thus, total membrane order arises through a distinct population of saturated phospholipids with mostly trans acyl chain conformations (fig. S10C). The frequency of this population oscillates during successive sterol modifications in the post-synthetic steps.

One model for sterols ordering phospholipids is strictly through direct sterol-acyl chain interactions, which were envisioned initially

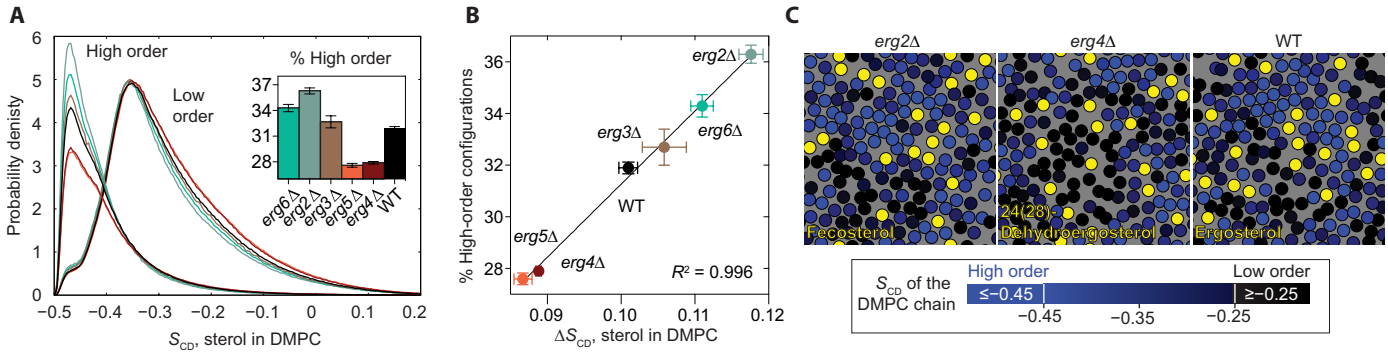

Fig. 7. Post-synthetic intermediates modulate long-range ordering of saturated phospholipids. (**A**) The frequency of the high-order DMPC populations, which contains mostly trans acyl chain conformers, increases in abundance with higher ordering sterols. Error bars and total distributions for each system and sterol-free DMPC are shown in fig. S10A. (**B**) The increase in higher order configurations tightly correlates with total ordering for each sterol system. Error bars = SD. (**C**) Sterol structural changes manifest in long-range ordering of DMPC. Panels show top-down view of the all-atom simulation with sterols, which are rendered as yellow circles, and DMPC chains, which are rendered as circles colored according to their order parameter as indicated in the key. Transient pockets of ordered DMPC acyl chains (blue) are observed in all systems but are most extensive in the solid-domain forming fecosterol (left) and least extensive in sterols that do not allow for demixing, like 24(28)-dehydroergosterol (middle). Ergosterol (right), which supports fluid domains, shows an intermediate level. Movies S1 and S2 show the dynamics of these components during simulation and further illustrate the differences between these three systems. In movie S2, DMPC acyl chains are color coded by S_{CD}, while, in movie S1, they are a uniform coloring to better highlight dynamics.

by Bloch. However, in our simulations, DMPC chains outnumber sterols 8:1, so the frequency of induced ordered chains that we observed was in stoichiometric excess of the sterol (Fig. 7A, inset). Thus, the effect of changing sterol structure manifests in long-range ordering within the system. An explanation of this paradox lies in the assembly of transient, hexagonally packed regions of saturated acyl chains, which were previously observed in simulations of L_o regions of ternary lipid mixtures that phase separate (*37*, *38*). These structures are seen in movies showing simulation trajectories of DMPC chains in sterol-containing systems (movie S1). We further characterized hexagonal by quantifying the distribution of DMPC chains and their individual S_{CD} values as a function of radial distance from sterols (fig. S11A). This analysis showed that DMPC ordering differences between sterol systems were constant with regards to distance from the sterol (fig. S11B), consistent with long-range ordering. High-order sterols in the pathway, like fecosterol in the *erg2*Δ systems, led to systems with more extensive hexagonal DMPC packing without a clear signal of enhanced ordering near the sterol (fig. S11C). In contrast, systems with no or only low-ordering sterols, like 24(28)-dehydroergosterol in *erg4*Δ, had few such structures. Ergosterol (WT) caused regions of dense hexagonal packing and other regions of disorder (Fig. 7C and movie S2), which corresponded to an intermediate level of DMPC ordering across the system (Fig. 7A) and surrounding the sterol (fig. S11C). These features correspond with the ergosterol's capacity to support ordered domains that remain fluid.

DISCUSSION

Here, we explored the biophysical driving forces underlying a single metabolic pathway through a combination of in vivo, in vitro, and in silico approaches. Previous comparisons between sterols have largely focused on a small number of natural or synthetic sterols. We capitalized on the ability of yeast cells to remain viable while accumulating intermediates across the ergosterol pathway to perform a systematic analysis. The resulting strains (table S1) are broadly useful for systematic investigation of sterol function. Here, we used domain formation of the yeast vacuole as a cellular readout of a sterol-dependent property (membrane phase separation), generating structure-predictions that could be tested by model membrane experiments and through simulations. These additional approaches are important because our analysis of sterol composition in vivo did not measure their abundance in the vacuole membrane, which is controlled by trafficking, or account for potentially compensatory changes in other lipid components. These might explain why some behaviors observed in synthetic vesicles, like gel-like domains caused by early post-synthetic intermediates, were not observed in vacuoles. Cellular measurements also cannot detect nanoscopic domains due to resolution constraints common to live cell imaging. In contrast, in vitro measurements do not account for membrane complexity in cells, like inter-leaflet asymmetry that has been recently shown to affect domain-formation capacities of sterol intermediates (*39*). Nonetheless, we found agreement between several observations made in vacuoles and the propensity of extracted intermediates to support domain formation in vesicles, and all sterols that supported uniform domains in the former yielded L_o/L_d phase separation in the latter. We also used sterol extracts from mutants to characterize the ordering capacity of post-synthetic intermediates, which agreed with all-atom simulations based on sterol models built with permutations from the metabolic pathway. Analysis of simulations showed that unsaturations in the sterol B-ring and alkyl tail are potent modulators of ordering capacity, which manifests through nanometer-scale hexagonal packing of saturated chains, as previously observed in simulated L_o phases (*37*, *38*). That is, total order is a measure of the sterol's ability to promote the collective structure of the ordered phase, rather than acting completely locally.

Our experimental design was motivated by the Bloch hypothesis, which postulated that the evolution of long metabolic pathways for sterols would have required a progression of biophysical fitness along the pathway. We find that the ergosterol pathway matches the criteria laid out by Bloch, but not for phospholipid condensation as

originally proposed. Instead, the pathway acts to generate a final product that can interact with phospholipids in a manner that supports phase separation of coexisting fluid domains. Counterintuitively, it does so by reducing the condensation capacity of its final product, ergosterol. Initial demethylated sterols, like zymosterol and fecosterol, provide too much order and drive the formation of solid domains in model membranes. In simulations, these intermediates show a smooth-faced ring system (Fig. 6A), cause a high abundance of phospholipids with all trans acyl chain isomers (Fig. 7B), and promote extensive hexagonal packing that is consistent with the nucleation of solid domains (Fig. 7C). The pathway subsequently acts to reduce condensation capacity through the Δ^8 isomerase Erg2 and further through two additional desaturases acting at the B-ring (Erg3) and alkyl tail (Erg5). This generates a series of intermediaries with poor ordering capacity and an inability to support any phase separation. These low-order sterols, like penultimate intermediate 24(28)-dehydroergosterol, feature a rougher ring system and promote only low levels of long-range ordering compared to earlier intermediates. The final step of the pathway, carried out by the reductase Erg4, generates a saturated methyl group at the alkyl tail, which partially recovers ordering capacity in ergosterol and the two other intermediates (ergosta-5,7-dienol and ergosta-7,22-dienol) that support phase separation in both vacuoles and GUVs. These Erg4 products still show low ordering capacity for unsaturated lipids while retaining an intermediate ordering capacity for saturated lipids (Figs. 5 and 6B).

Compared to all its precursors, we find that ergosterol optimizes the phase separation of membranes into coexisting liquid phases. Previously, it was assumed that formation of L_o domains correlated with a sterol's capacity to order phospholipids (*20*). However, the capacity of ergosterol to form ordered domains, despite its modest ordering capacity, has been unexplained (*40*). In yeast cells, phase separation of membrane domains is required for cell survival, as it underlies micro-autophagy in the vacuole (*23*, *41*). Similar processes have been proposed to act in numerous biological processes in other cell types (*42*, *43*). Unlike condensation capacity, formation of liquid domains depends on sterols and their interactions with at least two other classes of lipids, e.g., unsaturated and saturated phospholipids with low and high melting temperatures (*16*). Membrane phase separation requires sufficient line tension between two coexisting phases (*44*, *45*), which is related to their thickness differences (*46*–*48*). Consistent with these models, we observe that ergosterol still supports a large ordering difference between unsaturated (POPC) and saturated (DMPC) phospholipids. A challenge for biologically relevant membrane phase separation, however, is achieving such ordering differences while preventing domains from falling below their melting temperature. While ergosterol's moderate ordering capacity supports liquid phase separation, early demethylated precursors (zymosterol and fecosterol) that induce higher ordering instead drive formation of solid domains. This dynamic could explain why ordering capacity must be tuned down by post-synthetic steps in the ergosterol pathway. The exact molecular mechanism that favors the formation of hexagonally packed nanometer-scale domains into a fluid phase versus a solid or gel-like phase is still unclear, but it could require a delicate balance between sterol ordering capacity and affinity for the ordered chains. Our simulations suggest that solid domains are characterized by more extensive hexagonal packing with overall higher ordering. Future simulations that are expanded in both size and compositional space may enable a comparison of the molecular structure of different types of ordered phases observed experimentally.

As Bloch first proposed, the properties of sterol intermediates carry implications for the evolution of sterol metabolism in eukaryotes. In the initial steps of sterol metabolism, an ability of linear precursors, squalene and 2,3-oxidosqualene, to promote membrane heterogeneity (Fig. 2, C and E) suggests that they could have served early roles in membrane organization. The synthesis of these terpenes and their cyclization into lanosterol could have acted to promote or reduce gel-like domains, respectively, alongside sphingolipids. Conserved modifications, which demethylate lanosterol into zymosterol, would have been selected for in the last common ancestor of eukaryotes due to the elevated membrane stability and reduced permeability provided by demethylated sterols, as postulated by Bloch. The high ordering capacity of early ergosterol precursors, like fecosterol, could also explain why their accumulation has been selected for in laboratory evolution experiments at high temperatures that, otherwise, reduces membrane ordering (*49*). In the post-synthetic steps, a requirement for functional membrane organization would have driven the multistep adoption of ergosterol, which has reduced ordering capacity compared to zymosterol but allows for L_o/L_d phase separation. Within the post-synthetic steps, the promiscuity of Erg4's C24(28) reductase activity and its capacity to support domains in both *erg3*Δ and *erg5*Δ backgrounds suggests that it might have evolved before Erg3 and Erg5's desaturase activity. In this way, fluid membrane domains would have arisen before the adoption of ergosterol as a final product, even if the direct precursors of ergosterol in the extant pathway do not support them. In this putative proto-pathway (a sequence of Erg6-Erg2-Erg4-Erg3-Erg5), successive final products during the pathway's evolution would have initially supported solid domains, followed by a series of increasingly robust fluid domains.

While ergosterol is the dominant sterol across fungi, metazoan and plant sterols can also support phase separation both in model systems and in cells. The biosynthetic pathway for cholesterol, which Bloch first characterized, shows intriguing similarities and differences from that of ergosterol. Both cholesterol and ergosterol metabolism feature a Δ^8 isomerase step that buffers the capacity of their shared early intermediates to form solid domains and late-pathway reductases that are essential for generating a product that supports phase separation (*19*). Previously, it was observed that some cholesterol intermediates, like the Δ^7 intermediate lathosterol, show a higher capacity to stabilize saturated lipid domains (*50*). These measurements were taken using fluorescence quenching upon nanoscale organization, so they could not discern between L_o and solid domains, but they suggest that nonlinearity in condensation capacity might be shared across sterol metabolic pathways. Lathosterol also shows a lower solubility in DPPC bilayers (*51*), further suggesting that it could favor solid domains like post-synthetic ergosterol intermediates do, although this has not been directly tested.

How and why different sterol metabolic pathways diverged remains an open question, but their evolution suggests multiple chemical solutions to achieve membrane organization. The C24 methylation that is found in ergosterol and some plant sterols is absent from cholesterol metabolism, and so these late-stage reductases act on different positions, e.g., C24 (*25*) and at the B-ring. Enzymatic promiscuity is common in sterol metabolism; switching between two sterols can even occur via single step changes much earlier in pathways (*52*). Generation of new sterols could have thus occurred rapidly during

early eukaryotic evolution, potentially in response to the diversification of other membrane components, like sphingolipids whose chemistry also varies across lineages (*12*, *50*). In this way, the radiation of sterol metabolism could have also been driven by the need to balance interactions with other lipids.

MATERIALS AND METHODS

Yeast strains, plasmids, and media

Saccharomyces cerevisiae W303a was the base strain for the study. Knockout strains were generated by polymerase chain reaction–based homologous recombination. For knockdown strains except those targeting *ERG7*, a tetO2-*CYC1* promoter and expression cassette for the tetracycline-controlled transactivator were amplified from plasmid PCM224 and substituted upstream from the start codon of the gene of interest. For *ERG7* promoter substitution, the *MET3* promoter was used instead. All strains generated are listed in table S1. For visualization of vacuole domains in vivo, yeast strains were transformed with plasmid pRS426 GFP-Pho8. For strain generation, cells were grown in yeast extract, peptone, and dextrose (YPD) medium (Thermo Fisher Scientific), buffered complete supplement mixture (CSM; 0.5% w/v ammonium sulfate, 0.17% yeast nitrogen base without amino acids, 80 mM potassium phosphate dibasic, and 2% glucose), and buffered minimal medium (0.5% ammonium sulfate, 0.17% yeast nitrogen base without amino acids, 80 mM potassium phosphate dibasic, and 0.4% glucose).

Analysis of vacuole membrane domains

Vacuole membrane domain formation was induced by glucose depletion, and cells were subsequently imaged by confocal microscopy, as described previously (*53*). Briefly, a starter culture harboring the pRS426 GFP-Pho8 plasmid is grown in 5 ml of YPD overnight then diluted 1:100 into 5 ml of CSM medium lacking uracil for selection and incubated for 16 to 18 hours. Approximately 0.1 optical density (OD) unit of the CSM culture was diluted in 5 ml of minimal medium containing 0.4% glucose and lacking uracil and incubated for 24 hours before imagining. For *ERG* knockdowns under control of the $tetO_2$-*CYC1* promoter, a stock solution (10 mg/ml) of doxycycline (Sigma-Aldrich) was added to the minimal medium to a final concentration between 100 and 500 ng/ml. For *ERG7* a 1000× (20 g/ml) methionine stock solution (Sigma-Aldrich) was added to the minimal medium at a final concentration of 2× (40 mg/ml). Cells grown in minimal medium were transferred to eight-well microscope chamber slides (Nunc Lab-Tek) pre-coated with concanavalin-A (1 to 2 mg/ml; MP Biomedicals). Vacuoles were imaged using a Zeiss LSM 880 Airyscan microscope at room temperature with a Plan-Apochromat 63×/1.4 oil differential interference contrast M27 objective. GFP excitation was via a 488-nm Argon laser at 2% power. Images were processed in Zen Black using default Airyscan settings. Vacuoles were captured from top to bottom, and three-dimensional projections were generated from processed Airyscan images using the Z project tool in ImageJ. All vacuoles in large fields of cells were manually assigned as having different domain classes (uniform, nonuniform, and no domains) as previously described (*53*): Uniform vacuoles do not show regions that exclude Pho8-GFP below the resolution limit of Airyscan microscopy, uniform domain vacuoles contain a hexagonal arrangement of domains that span the entire vacuole surface, and nonuniform domain vacuoles contain domains that are only in part of the vacuole surface; these also do not show hexagonal features of the uniform domains. A minimum of 100 cells were quantified in each biological replicate. Analysis of domain size was performed using Weka segmentation (*54*) using a training set of individual vacuole micrographs manually annotated into three classes (background, L_o domain, and L_d domain/Pho8-GFP). Perimeters of segmented domains were measured by the ImageJ analyze particle tool.

Cellular sterol extraction and analysis

Extraction of sterols from yeast has been described previously (*55*). Briefly, an amount of cells corresponding to an absorbance of 1 at OD_{600} was spiked with internal standard (cholesterol) and resuspended in 1 ml of Milli-Q water. Glass beads (1 ml) were added to break apart the cells, and the resulting cell lysate was then transferred to a 15-ml conical glass with a Teflon cup. Methanolic KOH (3 ml) was added. The resulting mixture was incubated at 70°C for 2 hours. The mixture is allowed to cool and 3 ml of *n*-hexane was added. The mixture was then mixed with a vortex at the highest setting for 10 s. The tube was then spun at room temperature by centrifugation for 5 min at 800 rpm. The upper organic phase was then transferred to a clean conical glass tube. A second extraction of the aqueous phase was performed, and the resulting organic phase was combined. The *n*-hexane was evaporated under a stream of nitrogen. The resulting dry extract was then dissolved in a 1:1 solution of pyridine and trimethylchlorosilane and incubated at 70°C for 1 hour for derivatization. Extracts were analyzed by gas chromatography–mass spectrometry (GC-MS) as follows. Samples were injected into a 30-m DB-5 column in an Agilent 8890 GC coupled to a 5977B mass analyzer. The GC oven was operated with the following temperature program: initial temperature of 120°C held for 1 min, ramped at 20°C per min to 270°C, followed by an additional ramp at 2°C per min to 290°C, and then a final ramp at 20°C per min to 300°C and held for 2 min. The identities of target compounds were initially checked against the NIST17 mass spectral library using NIST MS Search software. Mass spectra from the literature were used as an additional source when target compounds could not be found in the library. For quantification, sterol levels were calculated relative to a calibration curve of a cholesterol external standard and adjusted according to the extraction efficiency for each sample. Extraction efficiency was determined on a percent recovery basis of internal standard per sample.

Generation and analysis of sterol extracts

A starter culture in 5 ml of CSM was prepared and grown in a shaker for 24 hours, and the culture was diluted 1/100 into a final volume of 50 ml with fresh CSM in a 250-ml flask. After 24 hours of incubation, the culture was diluted 1/100 into a final volume of 650 ml with fresh CSM in a 2-liter non-baffled flask shaking at 200 rpm for 24 hrs. Cells were harvested by benchtop centrifugation (3000*g* for 20 min). Cells were washed with 650 ml of MQ water, then resuspended again in 650 ml of MQ, and aliquoted into 50-ml falcon tubes. Unused cells were spun down again (3000 rpm for 10 min), and MQ water was removed and stored in the −80°C for future use. For cells that were to be used immediately, 5 ml of resuspended cells were transferred into a 15-ml falcon tube for sterol extraction as described above with modifications. After alkaline hydrolysis, the unsaponified fraction was extracted with hexane. An additional cleanup step was performed to reduce the amount of non-sterol lipids present in the unsaponifiable fraction as described elsewhere (*56*). Briefly, the unsaponified fraction was mixed in a solvent mixture of additional

hexane, acetone, and methanol such that the composition was 72% (v/v) hexane, 14% (v/v) acetone, and 14% (v/v) methanol. This mixture was extracted in a separatory funnel with a solvent mixture consisting of 39.6% (v/v) hexane, 17.82% acetone, 41.58% methanol, and 1% (v/v) water. After separation, the upper organic phase was concentrated by rotary evaporation. The resulting lipid film was resuspended in 2 ml of chloroform and stored in an airtight container (Avanti Polar Lipids, 600511) at −20°C until use. Extracts were quantified by GC-MS, as described above, and quantified using an ergosterol external standard. GUVs and liposomes from sterol extracts were prepared as described above.

Giant vesicle electroformation

PC (Avanti Polar Lipids), ergosterol (Thermo Fisher Scientific), squalene (Echelon Biosciences), squalene (Sigma-Aldrich), 2,3-oxidosqualene (Sigma-Aldrich), GluCer C16 (Avanti Polar Lipids), lanosterol (Avanti Polar Lipids), FF-MAS (Avanti Polar Lipids), and Texas Red DHPE (Life Technologies) were used as purchased without further purification. Lipid solutions in chloroform typically contained DPPC (16:0 PC), ergosterol, and 0.8 mol % Texas Red DHPE, a dye that selectively partitions to the L_d phase. GUVs were electroformed in 200 mM sucrose, and 0.25 mg of lipids in stock solutions were spread evenly on slides coated with indium tin oxide (Delta Technologies). Lipid-coated slides were placed under vacuum for >30 min to evaporate the chloroform. A capacitor was created by sandwiching an O-ring (Ace Glass, 7855-14) between two lipid-coated slides, filling the gap with sucrose solution. An ac voltage of 10 Hz and 1.3 V was applied across the capacitor for 1 hour at 60°C. GUVs were harvested and allowed to cool at room temperature for 1 hour to allow domains to form and coalesce. Phase separation was assessed by imagining under wide-field fluorescence microscopy (Thermo EVOS equipped with 63× Nikon oil-immersion objective). Between 10 and 25 GUVs for each preparation were classified manually during extended visualization as either containing a single (coalesced) domain, multiple discrete domains that did not coalesce after 1 hour, or domains with rough/non-round morphologies. The latter two were classified as solid or gel like. GUVs with uniform distribution of Texas Red were classified as having no domains.

Fluorescence spectroscopy

Liposomes for spectroscopy were generated by thin film hydration at 50°C and extruded 21 times through 100-nm filters (Avanti Polar Lipids). Steady-state fluorescence readings were performed on a Cary Eclipse fluorometer (Agilent) equipped with automated polarizers. GP of Laurdan (Invitrogen, D250) was calculated from emission intensities at 440 and 490 nm upon excitation at 365 nm in liposome suspensions extruded to 100 nm and stained with 50 μM of the dye. Anisotropy of DPH (Sigma-Aldrich, D20800) was calculated from emission at 430 nm upon excitation at 360 nm in liposomes stained with 50 μM of the dye. All measurements were taken at 30°C. For estimation of T_{misc}, DPH anisotropy values were obtained across a temperature range (T) of 8° to 70°C and fitted to a Boltzmann sigmoidal equation

$$R = R_{min} \frac{R_{max} - R_{min}}{1 + e^{\frac{(T_{misc} - T)}{a}}}$$

where R refers to the DPH anisotropy ratio; R_{min} and R_{max} are the minimum and maximum fluorescence, respectively; T is the temperature; T_{misc} is the miscibility temperature; and a is the fitted slope.

Molecular dynamics simulations

Except for ergosterol itself, simulated ergosterol precursors models are named by the genetic change that would result in its upregulation, assuming the pathway in Fig. 3A, as opposed to their chemical name. Systems were built using the CHARMM-GUI web module with ergosterol precursors substituted for ergosterol as needed. Parameters and chargers were chosen by analogy to similar chemical structures in the CHARMM C36 lipid force field. In the one case where parameters were not obviously transferrable [the diene torsion of 24(28)-dehydroergosterol in *erg4*Δ models], dihedral parameters were fit to a model compound [the tail of 24(28)-dehydroergosterol] using the MP2/6-31G* quantum chemical method and the Q-Chem 5.0.1 software package. Each system was initially equilibrated using the standard steps of the CHARMM-GUI package using the molecular dynamics package NAMD. Subsequent equilibration and production were performed with AMBER 20 on a single A100 GPU. Standard simulation parameters were used appropriate for the C36 force field (Lennard-Jones forces were switched off between 10 and 12 Å, the particle mesh Ewald method was used to compute long range electrostatics, and bonds to hydrogen were constrained using SHAKE/SETTLE). Temperature was maintained at 30°C using a Langevin thermostat. Isotropic 1-atm pressure at zero lateral tension was maintained using AMBER's Monte Carlo barostat. Systems were run at 20 mol % sterol in DMPC (20 sterol molecules and 80 phospholipids per leaflet) for at least 500 ns each, in triplicate, with the initial 100 ns neglected. Approximately 10,000 water molecules were used per system, consistent with the default hydration recommended by CHARMM-GUI.

Sterol tail conformation analysis

Tail conformations were identified by first constructing histograms of each independent dihedral angle of a sterol tail. Stable dihedral basins with significant likelihood were unambiguous. Each basin of each dihedral was assigned a discrete number, enabling enumeration of all possible tail conformational states. For each frame of simulation analysis, the instantaneous total bilayer order was correlated with the instantaneous number of each tail conformation. For example, the most likely tail conformation of ergosterol [44%; C13-C17-C20-C22, 176°; C17-C20-C22-C23, 239°; C22-C23-C24-C25, 117°; and C23-C24-C25-C26, 291°] had correlation $\rho = 0.056$ with the order parameter. The impact on overall order ΔS_{CD} from conformation i was estimated as

$$\Delta S_{CD} \approx f_i \frac{n_{sterol} \rho_i \sigma_s}{\sigma_i}$$

where σ_s is the SD of the order parameter, f_i is the average fraction of sterol with conformation i, σ_i is the SD of $n_{sterol} f_i$, and ρ_i is the correlation of bilayer order with the number ($n_{sterol} f_i$) of conformations i. This is equivalent to a least-squares linear fit to the order as a function of the total number of tail conformations, evaluated at the observed number of tail conformations. Data for conformations with >1% fraction are reported in data S1.

Acyl chain population analysis

For all the systems, the 10 dihedral angles from the DMPC acyl chains (carbons 2 to 14) were computed. Dihedrals with absolute angles smaller than 115° were considered gauche (G), others trans (T). Each acyl chain was then assigned a 10-letter code with either G or T in each position. The percentage of each code was computed for

all systems (data S2), revealing a monotonic increase of codes XTT TTTTTTX, TGTTTTTTTX, TTTTTTTTGX, and TTTTTTTGTG (total of 10) with increasing order. The distribution of order parameters (S_{CD}) for those configurations was then generated for each system, showing a significant contribution to the high order peak of DMPC acyl chains, which again increased with order (fig. S10).

Distance-dependent ordering analysis

To identify the distance dependence in the ordering effect of the different sterols, we computed two functions quantifying acyl chains relative to a sterol molecule. The first is the radial distribution function (RDF) between the DMPC acyl chains and the sterol molecules. This was computed as

$$\mathrm{RDF}(r_n) = \frac{1}{N_F}\sum_{f=1}^{N_F}\frac{\overline{A}}{N_a N_s}\frac{1}{(2n+1)\pi\Delta r^2}\sum_{i=1}^{N_s}\sum_{j=1}^{N_a} 1_{|r_i - r_j|\in(r_n, r_n+\Delta r)}$$

The equation above is used to compute the RDF for any distance $r_n = n\Delta r$ for a trajectory with N_F frames, containing N_s sterol molecules and N_a DMPC acyl chains ($N_a/2$ DMPC molecules). We here used the radial interval $\Delta r = 0.1$ Å.

To further investigate the distance dependence, we computed a second function that we call the average radial DMPC acyl chain S_{CD} (or RS_{CD})

$$RS_{\mathrm{CD}}(r_n) = \frac{\sum_{f=1}^{N_F}\sum_{i=1}^{N_s}\sum_{j=1}^{N_a} S_{CDf,j} * 1_{|r_i - r_j|\in(r_n, r_n+\Delta r)}}{\sum_{f=1}^{N_F}\sum_{i=1}^{N_s}\sum_{j=1}^{N_a} 1_{|r_i - r_j|\in(r_n, r_n+\Delta r)}}$$

This second function is computed in the same manner as the first, but S_{CD} is averaged across varying distances.

Supplementary Materials

The PDF file includes:

Figs. S1 to S11
Table S1
Legends for movies S1 and S2
Legends for data S1 to S3
References

Other Supplementary Material for this manuscript includes the following:

Movies S1 and S2
Data S1 to S3

REFERENCES AND NOTES

1. S. L. Regen, Cholesterol's condensing effect: Unpacking a century-old mystery. *JACS Au* **2**, 84–91 (2022).
2. J. Henriksen, A. C. Rowat, E. Brief, Y. W. Hsueh, J. L. Thewalt, M. J. Zuckermann, J. H. Ipsen, Universal behavior of membranes with sterols. *Biophys. J.* **90**, 1639–1649 (2006).
3. J. J. Brocks, B. J. Nettersheim, P. Adam, P. Schaeffer, A. J. M. Jarrett, N. Güneli, T. Liyanage, L. M. van Maldegem, C. Hallmann, J. M. Hope, Lost world of complex life and the late rise of the eukaryotic crown. *Nature* **618**, 767–773 (2023).
4. W. R. Nes, W. D. Nes, "Phylogenetics and biosynthesis" in *Lipids in Evolution*, W. R. Nes, W. D. Nes, Eds. (Springer, 1980), pp. 157–192.
5. K. Bloch, *Blondes in Venetian Paintings, the Nine-Banded Armadillo, and Other Essays in Biochemistry* (Yale Univ. Press, 1994).
6. P. L. Yeagle, R. B. Martin, A. K. Lala, H. K. Lin, K. Bloch, Differential effects of cholesterol and lanosterol on artificial membranes. *Proc. Natl. Acad. Sci. U.S.A.* **74**, 4924–4926 (1977).
7. C. E. Dahl, J. S. Dahl, K. Bloch, Effect of alkyl-substituted precursors of cholesterol on artificial and natural membranes and on the viability of Mycoplasma capricolum. *Biochemistry* **19**, 1462–1467 (1980).
8. K. E. Bloch, Sterol structure and membrane function. *CRC Crit. Rev. Biochem.* **14**, 47–92 (1983).
9. K. E. Bloch, Speculations on the evolution of sterol structure and function. *CRC Crit. Rev. Biochem.* **7**, 1–5 (1979).
10. T. Róg, M. Pasenkiewicz-Gierula, I. Vattulainen, M. Karttunen, What happens if cholesterol is made smoother: Importance of methyl substituents in cholesterol ring structure on phosphatidylcholine-sterol interaction. *Biophys. J.* **92**, 3346–3357 (2007).
11. J. D. Weete, M. Abril, M. Blackwell, Phylogenetic distribution of fungal sterols. *PLOS ONE* **5**, e10899 (2010).
12. Y.-T. Tsai, W. Moore, H. Kim, I. Budin, Bringing rafts to life: Lessons learned from lipid organization across diverse biological membranes. *Chem. Phys. Lipids* **233**, 104984 (2020).
13. C. Bernsdorff, R. Winter, Differential properties of the sterols cholesterol, ergosterol, β-sitosterol, trans-7-Dehydrocholesterol, stigmasterol and lanosterol on DPPC bilayer order. *J. Phys. Chem. B* **107**, 10658–10664 (2003).
14. S. Dupont, G. Lemetais, T. Ferreira, P. Cayot, P. Gervais, L. Beney, Ergosterol biosynthesis: A fungal pathway for life on land? *Evolution* **66**, 2961–2968 (2012).
15. G. L. Nicolson, Update of the 1972 singer-Nicolson fluid-mosaic model of membrane structure. *Discoveries* **1**, e3 (2013).
16. S. L. Veatch, S. L. Keller, Separation of liquid phases in giant vesicles of ternary mixtures of phospholipids and cholesterol. *Biophys. J.* **85**, 3074–3083 (2003).
17. M. B. Sankaram, T. E. Thompson, Deuterium magnetic resonance study of phase equilibria and membrane thickness in binary phospholipid mixed bilayers. *Biochemistry* **31**, 8258–8268 (1992).
18. M. E. Beattie, S. L. Veatch, B. L. Stottrup, S. L. Keller, Sterol structure determines miscibility versus melting transitions in lipid vesicles. *Biophys. J.* **89**, 1760–1768 (2005).
19. G. Staneva, C. Chachaty, C. Wolf, P. J. Quinn, Comparison of the liquid-ordered bilayer phases containing cholesterol or 7-dehydrocholesterol in modeling Smith-Lemli-Opitz syndrome. *J. Lipid Res.* **51**, 1810–1822 (2010).
20. X. Xu, E. London, The effect of sterol structure on membrane lipid domains reveals how cholesterol can induce lipid domain formation. *Biochemistry* **39**, 843–849 (2000).
21. I. Levental, K. R. Levental, F. A. Heberle, Lipid rafts: Controversies resolved, mysteries remain. *Trends Cell Biol.* **30**, 341–353 (2020).
22. A. Toulmay, W. A. Prinz, Direct imaging reveals stable, micrometer-scale lipid domains that segregate proteins in live cells. *J. Cell Biol.* **202**, 35–44 (2013).
23. T. Tsuji, M. Fujimoto, T. Tatematsu, J. Cheng, M. Orii, S. Takatori, T. Fujimoto, Niemann-Pick type C proteins promote microautophagy by expanding raft-like membrane domains in the yeast vacuole. *eLife* **6**, e25960 (2017).
24. S. P. Rayermann, G. E. Rayermann, C. E. Cornell, A. J. Merz, S. L. Keller, Hallmarks of reversible separation of living, unperturbed cell membranes into two liquid phases. *Biophys. J.* **113**, 2425–2432 (2017).
25. H. Kim, I. Budin, Intracellular sphingolipid sorting drives membrane phase separation in the yeast vacuole. *J. Biol. Chem.* **300**, 105496 (2023).
26. C. L. Leveille, C. E. Cornell, A. J. Merz, S. L. Keller, Yeast cells actively tune their membranes to phase separate at temperatures that scale with growth temperatures. *Proc. Natl. Acad. Sci. U.S.A.* **119**, e2116007119 (2022).
27. S. L. Veatch, S. L. Keller, Organization in lipid membranes containing cholesterol. *Phys. Rev. Lett.* **89**, 268101 (2002).
28. A. M. Polak, Preclinical data and mode of action of amorolfine. *Clin. Exp. Dermatol.* **17**, 8–12 (1992).
29. A. R. P. Varela, A. S. Couto, A. Fedorov, A. H. Futerman, M. Prieto, L. C. Silva, Glucosylceramide reorganizes cholesterol-containing domains in a fluid phospholipid membrane. *Biophys. J.* **110**, 612–622 (2016).
30. A. L. Munn, A. Heese-Peck, B. J. Stevenson, H. Pichler, H. Riezman, Specific sterols required for the internalization step of endocytosis in yeast. *Mol. Biol. Cell* **10**, 3943–3957 (1999).
31. M. Kato, W. Wickner, Ergosterol is required for the Sec18/ATP-dependent priming step of homotypic vacuole fusion. *EMBO J.* **20**, 4035–4040 (2001).
32. R. A. Fratti, Y. Jun, A. J. Merz, N. Margolis, W. Wickner, Interdependent assembly of specific regulatory lipids and membrane fusion proteins into the vertex ring domain of docked vacuoles. *J. Cell Biol.* **167**, 1087–1098 (2004).
33. A. Khmelinskaia, J. M. T. Marquês, A. E. P. Bastos, C. A. C. Antunes, A. Bento-Oliveira, S. Scolari, G. M. D. S. Lobo, R. Malhó, A. Herrmann, H. S. Marinho, R. F. M. de Almeida, Liquid-ordered phase formation by mammalian and yeast sterols: A common feature with organizational differences. *Front. Cell Dev. Biol.* **8**, 337 (2020).
34. W.-C. Hung, M.-T. Lee, H. Chung, Y.-T. Sun, H. Chen, N. E. Charron, H. W. Huang, Comparative study of the condensing effects of ergosterol and cholesterol. *Biophys. J.* **110**, 2026–2033 (2016).
35. T. T. Bui, K. Suga, H. Umakoshi, Ergosterol-induced ordered phase in ternary lipid mixture systems of unsaturated and saturated phospholipid membranes. *J. Phys. Chem. B* **123**, 6161–6168 (2019).

36. K. Hąc-Wydro, P. Wydro, M. Flasiński, The comparison of zymosterol vs cholesterol membrane properties – The effect of zymosterol on lipid monolayers. *Colloids Surf. B Biointerfaces* **123**, 524–532 (2014).
37. A. J. Sodt, M. L. Sandar, K. Gawrisch, R. W. Pastor, E. Lyman, The molecular structure of the liquid-ordered phase of lipid bilayers. *J. Am. Chem. Soc.* **136**, 725–732 (2014).
38. A. J. Sodt, R. W. Pastor, E. Lyman, Hexagonal substructure and hydrogen bonding in liquid-ordered phases containing palmitoyl sphingomyelin. *Biophys. J.* **109**, 948–955 (2015).
39. J. W. St Clair, E. London, Effect of sterol structure on ordered membrane domain (raft) stability in symmetric and asymmetric vesicles. *Biochim. Biophys. Acta Biomembr.* **1861**, 1112–1122 (2019).
40. X. Xu, R. Bittman, G. Duportail, D. Heissler, C. Vilcheze, E. London, Effect of the structure of natural sterols and sphingolipids on the formation of ordered sphingolipid/sterol domains (rafts). Comparison of cholesterol to plant, fungal, and disease-associated sterols and comparison of sphingomyelin, cerebrosides, and ceramide. *J. Biol. Chem.* **276**, 33540–33546 (2001).
41. A. Y. Seo, P.-W. Lau, D. Feliciano, P. Sengupta, M. A. L. Gros, B. Cinquin, C. A. Larabell, J. Lippincott-Schwartz, AMPK and vacuole-associated Atg14p orchestrate μ-lipophagy for energy production and long-term survival under glucose starvation. *eLife* **6**, e21690 (2017).
42. S. A. Shelby, I. Castello-Serrano, K. C. Wisser, I. Levental, S. L. Veatch, Membrane phase separation drives responsive assembly of receptor signaling domains. *Nat. Chem. Biol.* **19**, 750–758 (2023).
43. I. Castello-Serrano, F. A. Heberle, B. Diaz-Rohrer, R. Ippolito, C. R. Shurer, P. Lujan, F. Campelo, K. R. Levental, I. Levental, Partitioning to ordered membrane domains regulates the kinetics of secretory traffic. *eLife* **12**, RP89306 (2024).
44. A. J. García-Sáez, S. Chiantia, P. Schwille, Effect of line tension on the lateral organization of lipid membranes. *J. Biol. Chem.* **282**, 33537–33544 (2007).
45. R. D. Usery, T. A. Enoki, S. P. Wickramasinghe, M. D. Weiner, W.-C. Tsai, M. B. Kim, S. Wang, T. L. Torng, D. G. Ackerman, F. A. Heberle, J. Katsaras, G. W. Feigenson, Line tension controls liquid-disordered + liquid-ordered domain size transition in lipid bilayers. *Biophys. J.* **112**, 1431–1443 (2017).
46. J. V. Bleecker, P. A. Cox, R. N. Foster, J. P. Litz, M. C. Blosser, D. G. Castner, S. L. Keller, Thickness mismatch of coexisting liquid phases in noncanonical lipid bilayers. *J. Phys. Chem. B* **120**, 2761–2770 (2016).
47. J. V. Bleecker, P. A. Cox, S. L. Keller, Mixing temperatures of bilayers not simply related to thickness differences between L_o and L_d phases. *Biophys. J.* **110**, 2305–2308 (2016).
48. F. A. Heberle, R. S. Petruzielo, J. Pan, P. Drazba, N. Kučerka, R. F. Standaert, G. W. Feigenson, J. Katsaras, Bilayer thickness mismatch controls domain size in model membranes. *J. Am. Chem. Soc.* **135**, 6853–6859 (2013).
49. L. Caspeta, Y. Chen, P. Ghiaci, A. Feizi, S. Buskov, B. M. Hallström, D. Petranovic, J. Nielsen, Biofuels. Altered sterol composition renders yeast thermotolerant. *Science* **346**, 75–78 (2014).
50. Megha, O. Bakht, E. London, Cholesterol precursors stabilize ordinary and ceramide-rich ordered lipid domains (lipid rafts) to different degrees. Implications for the Bloch hypothesis and sterol biosynthesis disorders. *J. Biol. Chem.* **281**, 21903–21913 (2006).
51. M. G. K. Benesch, D. A. Mannock, R. N. A. H. Lewis, R. N. McElhaney, A calorimetric and spectroscopic comparison of the effects of lathosterol and cholesterol on the thermotropic phase behavior and organization of dipalmitoylphosphatidylcholine bilayer membranes. *Biochemistry* **50**, 9982–9997 (2011).
52. C. M. Souza, T. M. E. Schwabe, H. Pichler, B. Ploier, E. Leitner, X. L. Guan, M. R. Wenk, I. Riezman, H. Riezman, A stable yeast strain efficiently producing cholesterol instead of ergosterol is functional for tryptophan uptake, but not weak organic acid resistance. *Metab. Eng.* **13**, 555–569 (2011).
53. H. Kim, I. Juarez-Contreras, I. Budin, "Using the yeast vacuole as a system to test the lipidic drivers of membrane heterogeneity in living cells" in *Methods in Enzymology* (Academic Press, 2024).
54. I. Arganda-Carreras, V. Kaynig, C. Rueden, K. W. Eliceiri, J. Schindelin, A. Cardona, H. Sebastian Seung, Trainable Weka Segmentation: A machine learning tool for microscopy pixel classification. *Bioinformatics* **33**, 2424–2426 (2017).
55. Y. Gbelska, N. T. Hervay, M. Morvova Jr., A. Konecna, Sterol analysis in *Kluyveromyces lactis*. *Bio Protoc.* **7**, e2527 (2017).
56. A. A. Johansson, R. H. K. Kivikari, E. U. Suokas, Process for the separation of sterols, US Patent (1977).
57. D. Degreif, B. Cucu, I. Budin, G. Thiel, A. Bertl, Lipid determinants of endocytosis and exocytosis in budding yeast. *Biochim. Biophys. Acta Mol. Cell Biol. Lipids* **1864**, 1005–1016 (2019).

Acknowledgments: We thank E. Lyman and S. Keller for helpful discussions. **Funding:** This work was supported by the National Science Foundation (MCB-2046303 to I.B.), the National Institutes of Health (GM142960 to I.B., 1ZIAHD008955 to A.S., and T32-GM008326C to I.J.-C.), the Department of Energy (DE-SC0022954 to I.B.), and the intramural research program of the National Institute of Child Health and Human Development (L.J.S.L. and A.J.S.). Computational resources were provided by the National Institute of Child Health and Human Development and National Institutes of Health HPC Biowulf cluster. **Author contributions:** Conceptualization: I.J.-C., A.S., and I.B. Methodology: I.J.-C., L.J.S.L., A.S., and I.B. Investigation: I.J.-C., L.J.S.L., J.H., L.Y.-L., K.O., J.R.-R., and A.S. Visualization: I.J.-C., L.J.S.L., A.S., and I.B. Supervision: A.S. and I.B. Funding acquisition: A.S. and I.B. Writing—original draft: I.J.-C., L.J.S.L., A.S., and I.B. Writing—review and editing: I.J.-C., L.J.S.L., A.S., and I.B. **Competing interests:** The authors declare that they have no competing interests. **Data and materials availability:** All data needed to evaluate the conclusions in the paper are present in the paper and/or the Supplementary Materials. Datasets for all figures are archived at Zenodo (https://doi.org/10.5281/zenodo.14854037), as are molecular dynamics codes and trajectories used in the figures (https://doi.org/10.5281/zenodo.14962936). Sterol profiles for each strain are provided in data S3.

Submitted 24 November 2024
Accepted 19 March 2025
Published 23 April 2025
10.1126/sciadv.adu7190